Elucidation of stoichiometric efficiency, radical generation and transformation pathway during catalytic oxidation of sulfamethoxazole via peroxymonosulfate activation

Bao, Yueping; Oh, Wen-Da; Lim, Teik-Thye; Wang, Rong; Webster, Richard David; Hu, Xiao

2019

Bao, Y., Oh, W.-D., Lim, T.-T., Wang, R., Webster, R. D., & Hu, X. (2019). Elucidation of stoichiometric efficiency, radical generation and transformation pathway during catalytic oxidation of sulfamethoxazole via peroxymonosulfate activation. Water Research, 151, 64–74. doi:10.1016/j.watres.2018.12.007

https://hdl.handle.net/10356/143837

https://doi.org/10.1016/j.watres.2018.12.007

Elucidation of stoichiometric efficiency, radical generation and transformation pathway during catalytically oxidation of sulfamethoxazole via peroxymonosulfate activation

Yueping Bao [a,b], Wen-Da Oh [b,c], Teik-Thye Lim [b,d], Rong Wang [b,d], Richard David Webster [b,e], Xiao Hu [b,f*]

[a] *Interdisciplinary Graduate School, Nanyang Technological University, 637141, Singapore*

[b] *Nanyang Environment and Water Research Institute, Nanyang Technological University, 637141, Singapore*

[c] *School of Chemical Sciences, Universiti Sains Malaysia, 11800 Penang, Malaysia*

[d] *School of Civil and Environmental and Engineering, Nanyang Technological University, 639798, Singapore*

[e] *School of Physical and Mathematical Sciences, Nanyang Technological University, 637371, Singapore*

[f] *School of Materials Science and Engineering, Nanyang Technological University, 639798, Singapore*

* Corresponding author at: School of Materials Science and Engineering, Nanyang Technological University, Block N4.1, 50 Nanyang Avenue, Singapore 639798, Singapore.

Tel.: + 65 6790 4610

E-mail address: ASXHU@ntu.edu.sg.

Abstract

In this work, nano-bimetallic Co/Fe oxides with different stoichiometric Co/Fe ratios were prepared using a novel one-step solution combustion method. The nano-bimetallic Co/Fe oxides were used for sulfamethoxazole (SMX) degradation via peroxymonosulfate (PMS) activation. The stoichiometric efficiencies of the as-prepared nano-bimetallic catalysts were calculated and compared for the first time. The radical generation was identified by electron paramagnetic resonance (EPR) as well as chemical quenching experiments, in which different scavengers were used and compared. The catalytic PMS activation mechanism in the presence of catalyst was examined by Fourier transform infrared spectroscopy (FTIR) and X-ray photoelectron spectroscopy (XPS). The results showed that besides $SO_4\bullet^-$ and •OH, •OOH was also detected in the PMS/$CoFeO_{2.5}$ system. Meanwhile, in addition to the previously proposed radical oxidation pathway, the results showed that SMX degradation also involved a non-radical oxidation, which could be verified by the degradation experiment without catalyst as well as the detection of $^1O_2$. In the PMS activation process, cobalt functioned as the active site on $CoFeO_{2.5}$ while Fe oxide functioned as the adsorption site. The electron transfer mechanism was proposed based on the XPS and metal leaching results. Additionally, via the detection of transformation products, different SMX transformation pathways involving nitration, hydroxylation and hydrolysis in the PMS/$CoFeO_{2.5}$ system were proposed.

Keywords: nano-bimetallic oxides; stoichiometric efficiencies; peroxymonosulfate; radical generation; antibiotics; transformation pathway

1. Introduction

Sulfamethoxazole (4-amino-N-(5-methyl-3-isoxazolyl)-benzene sulfonamide, SMX) is one kind of widely used antibiotics due to its low cost and broad-spectrum antimicrobial ability (Jansomboon et al., 2016). The uncontrolled usage of SMX can have an undesired chronic effect on ecological system by inducing the appearance of antibiotic-resistant bacteria and genes (Rizzo et al., 2013). To date, SMX has been detected in various municipal sewage treatment plants, hospital effluents, surface water and even drinking water system (Godfrey et al., 2007; Lindberg et al., 2004; Nikolaou et al., 2007; Segura et al., 2009). Thus, it is necessary to conduct a comprehensive study for its transformation fate in the environment. Generally, SMX would be treated by various advanced oxidation processes because it cannot be removed effectively by the conventional treatment processes/technologies due to their biorecalcitrance (Alexy et al., 2004; Ryan et al., 2011). In recent years, sulfate radical-based advanced oxidation process (SR-AOP) has emerged as a potential solution for removing persistent organic pollutants in water (Zhang et al., 2015) due to its high redox potential of 2.60, wide pH flexibility (pH 1-9) (Fang et al., 2012) and high selective oxidation ability via electron transfer (Eberson, 1982; Hayon et al., 1972; Oh et al., 2016). It has been proven that the $SO_4^{\bullet -}$ radicals can be generated from peroxymonosulfate (PMS) via various activation methods (e.g., thermal, ultraviolet irradiation, ultra-sonication and catalytic activation) (Ghanbari and Moradi, 2017; Oh et al., 2017).

In the catalytic activation process, cobalt ion and its composites show high efficiency on PMS activation (Hu and Long, 2016). However, the observed undesirable Co leaching is one of the major concerns (Anipsitakis et al., 2005). On the other hand, iron ion plays a vital role during the catalytic reactions and the mixed metal oxides show better performances (Costa et al., 2006; Li et al., 2019; Miao et al., 2018). Several methods have been used for the synthesis of mixed metal oxides with multiple steps (Liang et al., 2014; Li et al., 2016). Meanwhile, in a

recent study, the Co/Fe bimetallic oxides with different stoichiometric ratios were synthesized for the activation of PMS to degrade norfloxacin, in which surface hydroxyl groups were proposed as the reason for higher efficiency and the sulfate radical dominated the degradation process (Chen et al., 2018). Yu et al. reported the synergism between Mn and Fe in a bimetallic oxide ($Mn_{1.8}Fe_{1.2}O_4$) for PMS activation for Bisphenol A (BPA) degradation, in which Fe works as the main adsorption site while Mn is the active site to generate radicals (Huang et al., 2017). Meanwhile, bimetallic oxides have also been used in PMS activation for SMX degradation (Bao et al., 2018a; Oh et al., 2017). However, the transformation mechanism of SMX especially the non-radical transformation pathway involved in this system is still unclear. Furthermore, the stoichiometric efficiencies of catalysts have rarely been calculated and reported.

Herein, a comprehensive transformation of SMX in PMS system in the presence of Co/Fe bimetallic oxides was explored. The SMX transformation pathways (i.e., non-radical pathway and radical pathway) as well as PMS activation mechanism were investigated. Meanwhile, the stoichiometric efficiencies of the as-prepared catalysts were calculated for the first time. Furthermore, the radical generation and electron transfer mechanism in the catalytic oxidation system were proposed.

2. Materials and Methods

2.1 Chemicals

All chemicals used in this study were reagent grade or higher and they were used without any further purification. All solutions were prepared at room temperature using deionized (DI) water (18.2 MΩ.cm at 25°C, Millipore system). Iron(III) nitrate nonahydrate ($Fe(NO_3)_3{\cdot}9H_2O$) was received from Acros organics. Cobalt(II) nitrate hexahydrate ($Co(NO_3)_2{\cdot}6H_2O$), sodium hydroxide (NaOH), nitrobenzene (NB, $C_6H_5NO_2$), benzoquinone (BQ, $C_6H_4O_2$), phenol (C_6H_6O), sodium azide (NaN_3), methanol (MeOH, CH_4O) and *tert*-

butanol (TBA, $C_4H_{10}O$) were purchased from Sigma-Aldrich. Urea (CH_4N_2O) was supplied by VWR and Oxone (PMS, $2KHSO_5 \cdot KHSO_4 \cdot K_2SO_4$) was provided by Alfa Aesar. 5,5-dimethyl-1-pyrrolidine N-oxide (DMPO) was purchased from Aladdin, 5-*tert*-Butoxycarbonyl-5-methyl-1-pyrroline-N-oxide (BMPO) was from Cayman Chemical and 2,2,6,6-tetramethylpiperidine (TEMP) was provided by Merck.

2.2 Nano-bimetallic Co/Fe oxides preparation and characterization

The nano-bimetallic Co/Fe oxides were synthesized via a novel one-step solution combustion method. In brief, a predetermined amount of $Co(NO_3)_2 \cdot 6H_2O$ and $Fe(NO_3)_3 \cdot 9H_2O$ were first dissolved in water followed by the addition of urea as the reductant. The detailed sample preparation is shown in Table S1. The as-prepared solutions were treated in a furnace at 400°C for 1 h to get the catalysts. The resulting catalysts are named as φ = x:y, where x:y is the molar ratio of Co and Fe.

The morphological and textural properties of the as-prepared catalysts were examined with a field emission scanning electron microscope (FESEM, JSM-7600F, JEOL, Japan) and X-rays diffractometer (XRD, Bruker D8 Advance) with a monochromated high intensity Cu-K_α (λ =1.54 Å) radiation. The specific surface areas of the catalysts were measured using the Brunauer-Emmett-Teller (BET) N_2 adsorption-desorption method with Quantachrome Autosorb -1 Analyzer. The valence states of the constituent elements were determined using X-ray photoelectron spectroscopy (XPS) (Kratos Axis Supra, Shimadzu) and the surface bonding properties of the catalysts and PMS were characterized using Fourier transform infrared spectroscopy (FTIR, Perkin Elmer).

2.3 Decomposition experiments

The SMX decomposition experiments were conducted in a batch system at room temperature unless otherwise stated. A certain amount of the as-prepared catalysts (10 mg) was dispersed into the SMX solution (40 μM, 50 mL). After that, a desired volume of PMS stock

126 solution (40 mM) was added into the mixture to initiate the degradation process. At pre-
127 determined sampling intervals, the mixture was collected and filtered through a 0.45 μm PTFE
128 filter immediately. To quench the residual radicals, an equal volume of methanol was injected
129 into the filtered samples before the detection (Oh et al., 2014; Yun et al., 2018). The initial pH
130 of SMX solution was 5 and was adjusted with 0.1 M NaOH solution if necessary. Meanwhile,
131 the quenching experiments were carried out by adding different scavengers prior to the PMS
132 (Table S2). The PMS self-decomposition experiments were conducted in the same condition
133 while without SMX.
134 *2.4 Analysis methods*
135 The concentration of PMS was measured using the KI colorimetric method with a UV-
136 1800 spectrophotometer (Shimadzu, Japan) at λ_{max} = 352 nm. The mass of metals leached
137 during the reaction was measured by inductively coupled plasma optical emission spectrometry
138 (ICP-OES, Optima 8000, Perkin Elmer). The concentration of SMX was measured using a
139 high-performance liquid chromatography system (LC-2030C 3D, Shimadzu) equipped with an
140 Inertsil ODS-3 column (4.6 × 150 mm; 5 μm). The UV detector was set at a wavelength of 264
141 nm and the mobile phases were composed of 60% A (methanol) and 40% B (0.1% acetic acid
142 water) at a flow rate of 0.8 mL min^{-1}. The intermediates were further analyzed using an Agilent
143 1290 Infinity HPLC coupled to an Agilent 6460 Triple quadruple mass spectrometry, which
144 was equipped with an Electrospray ionization (ESI) source using Agilent Jet Stream
145 Technology (Agilent, USA). The mobile phases consisted of water with 0.1% formic acid (A)
146 and acetonitrile with 0.1% formic acid (B), and the chromatographic separations were
147 performed with a 75 mm × 2 mm Luna 3μ C18 column. MS analyses were conducted with both
148 positive and negative modes (ESI^+/ESI^-) over a mass scan range of 50-400 m/z. For the
149 chromatographic separation, a gradient elution method with two mobile phases was employed
150 as follows: 90% A for 0-0.5 min; 90% A decreased to 10% A lineally for 0.5-5.5 min and kept

for 5.5-8.0 min; 10% A increased to 90% A lineally for 8.0-9.5 min and kept for 9.5-10.0 min. The flow rate was kept at 0.2 mL min^{-1}.

3. Results and discussion

3.1 Characterization of nano-bimetallic Co/Fe oxides

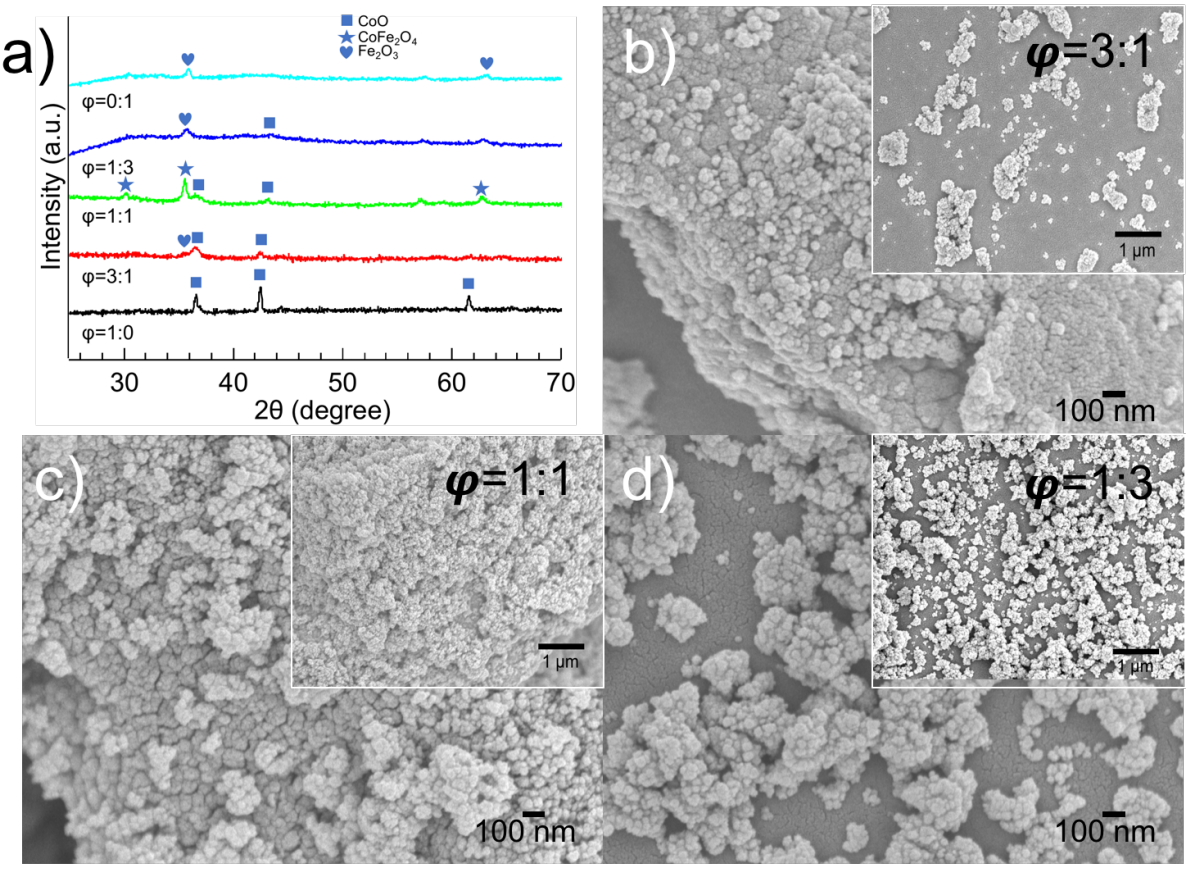

Fig 1. XRD patterns and FESEM images of nano-bimetallic Co/Fe oxides.

In the present study, three bimetallic oxides with different Co/Fe stoichiometric ratios (φ) were prepared (Fig 1). Meanwhile, the pure cobalt oxide and iron oxide were also prepared with a similar method for comparison (Fig S1). Fig 1a shows the XRD patterns of the as-prepared samples. The single metal oxides were identified as CoO (PDF. No. 96-154-1663) and Fe_2O_3 (PDF. NO. 96-901-2693), respectively. In all the bimetallic oxides, cobalt and iron would share the octahedral sites in the structure, resulting a mixed composites (Costa et al., 2006). Meanwhile, all particles consisted of irregular spherical nanoparticles with an average diameter of 50-200 nm (Figs 1 b-d). The nano-sized structures could cause the broad peaks in

XRD patterns (Fig 1a). Pure cobalt oxide shows a wire-like morphology while iron oxide shows a diamond shape with larger diameter (Fig S1). For bimetallic oxides, with the increasing of Co amount, the morphology changed from nanoparticles to rhombic nanosheets, which indicated that the stoichiometric ratio of Co/Fe affects the morphology of the products. Meanwhile, the bimetallic oxides show more porous and finer particles with increasing of Fe amount. The corresponding EDX spectra clearly demonstrated the presence of Fe, Co and O in the catalysts and the atomic ratios were close to the theoretical Co/Fe ratios, which were calculated as 3.09, 1.23 and 0.35 for φ=3:1, φ=1:1 and φ=1:3, respectively (Fig S2).

3.2 Catalytic decomposition of PMS in the presence of nano-bimetallic Co/Fe oxides

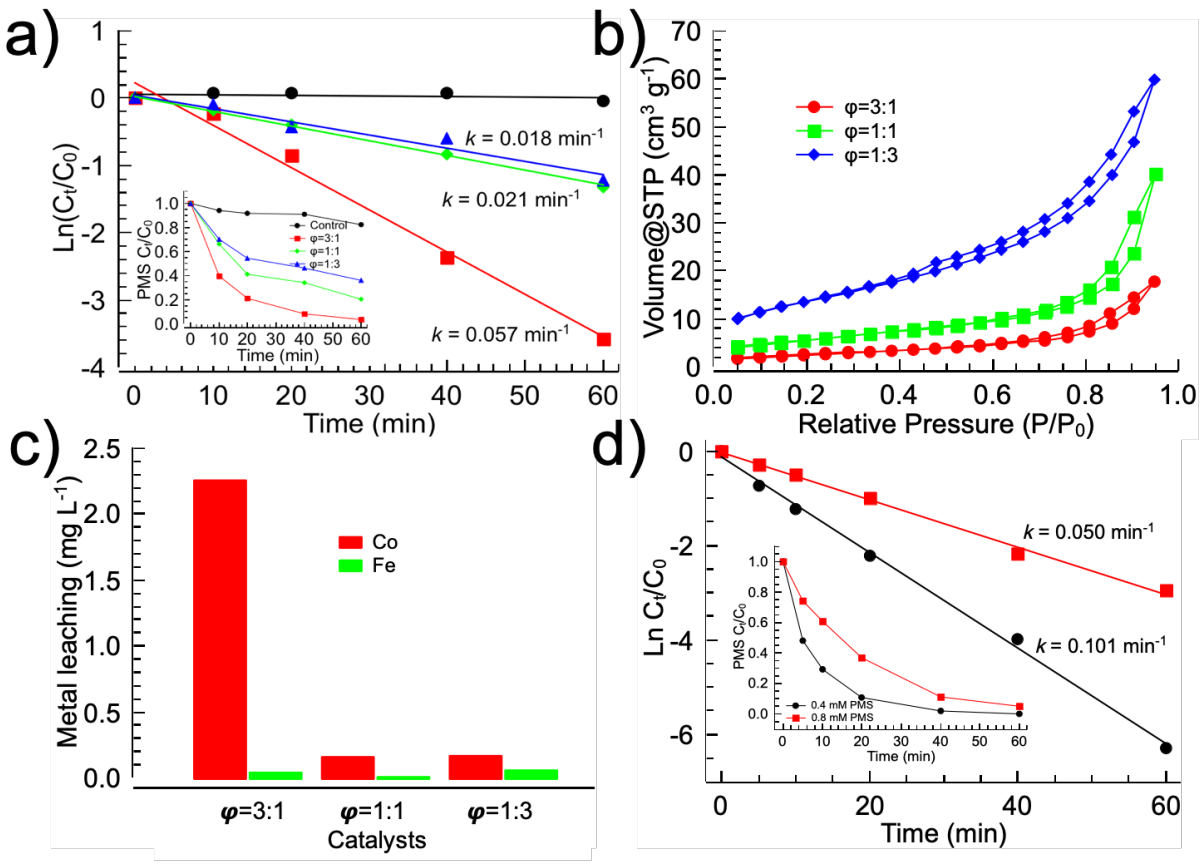

Fig 2. a) Catalytic decomposition of PMS in the presence of different nano-bimetallic Co/Fe oxides; b) the surface areas of as-prepared nano-bimetallic Co/Fe oxides; c) metal leaching test for different nano-bimetallic Co/Fe oxides and d) the PMS decomposition in

178 homogeneous system in the presence of Co^{2+} [Experimental Conditions: Catalyst = 0.2 g L^{-1}
179 and PMS = 0.4 mM for a, Co^{2+} = 2 mg L^{-1} for d].

180 As shown in Fig 2a, the PMS self-decomposition rate without catalyst was negligible
181 (<5%). In contrast, the heterogeneous system with nano-bimetallic Co/Fe oxides exhibited a
182 significantly accelerated PMS decomposition rate, with the $k_{obs\text{-}PMS}$ of 0.057, 0.021, 0.018 min^{-1}
183 for φ = 3:1, 1:1 and 1:3, respectively. To further examine the effect of different φ on the PMS
184 decomposition rate, the results were fitted with the following kinetics:

185 $$d\,[PMS] / d\,t = - k_{obs\text{-}PMS}\,[PMS] = - k_{SA\text{-}PMS}\,C_S\,[PMS] = - k_{SA\text{-}PMS}\,(S_S\,C)\,[PMS] \quad (1)$$

186 where $k_{obs\text{-}PMS}$ represents the observed pseudo-first-order rate constant (min^{-1}) in PMS
187 decomposition, $k_{SA\text{-}PMS}$ is the PMS decomposition rate constant normalized with the specific
188 surface area (L m^{-2} min^{-1}), Cs is the surface area of catalyst in solution (m^2 L^{-1}), S_S is the
189 specific surface area of catalyst (m^2 g^{-1}), and C is the catalyst loading amount (g L^{-1}). The
190 calculated results are shown in Table 1. The $k_{SA\text{-}PMS}$ of the catalysts followed the order φ = 3:1 >
191 φ = 1:1 > φ = 1:3. The nano-bimetallic Co/Fe oxides with φ = 3:1 has the highest PMS
192 decomposition rate, but it also shows the highest Co leaching (Table 1). Therefore, the higher
193 PMS decomposition rate for φ = 3:1 could be resulted from the contribution of leached Co^{2+} in
194 the solution instead of that of the catalyst. To verify this assumption, a homogeneous control
195 experiment with addition of Co^{2+} was conducted, which shows that Co^{2+} in the homogeneous
196 system possesses high activity in PMS decomposition (Fig 2d). For nano-bimetallic Co/Fe
197 oxides with φ = 1:1 and φ = 1:3, the metal leaching was much lower, which might be caused
198 by the formation of stronger interaction between Co and Fe (Table 1). In the present study, the
199 nano-bimetallic Co/Fe oxides with φ = 1:1 was selected for use in the following section. Based
200 on the EDX results, the chemical formula for φ = 1:1 is $CoFeO_{2.5}$, which could be a composite
201 of $CoFe_2O_4$ and CoO (Fig S2).
202

Table 1. Summary on the kinetic studies and metals leaching in PMS decomposition in presence of different nano-bimetallic Co/Fe oxides [PMS = 0.4 mM, reaction time = 60 min].

Catalysts	$k_{obs\text{-}PMS}$ (min^{-1})	$k_{SA\text{-}PMS}$ ($L\ m^{-2}\ min^{-1}$)	Cs ($m^2\ L^{-1}$)	BET S_S ($m^2\ g^{-1}$)	C ($g\ L^{-1}$)	Co ($mg\ L^{-1}$)	Fe ($mg\ L^{-1}$)
φ=1:0	0.138	--	--	< 2	0.2	15.9	--
φ=3:1	0.057	3.0×10^{-2}	1.9	9.5	0.2	2.26	0.04
φ=1:1	0.021	5.2×10^{-3}	4.1	20.3	0.2	0.16	0.01
φ=1:3	0.018	1.8×10^{-3}	9.8	49.2	0.2	0.17	0.06
φ=0:1	0.002	2.9×10^{-3}	0.7	3.5	0.2	--	0.01

3.3 Catalytic performance of $CoFeO_{2.5}$ in PMS activation for SMX degradation

Previously, it was reported that in the presence of organic contaminants, the radical chain decomposition of persulfate increased (Liu et al., 2014). However, in the present study, it was found that with the presence of SMX, the PMS decomposition rate decreased (Fig 3a). As shown in Fig 3b, with the increase of SMX concentration from 0-40 μM, the rate constant *k* for PMS decomposition decreased from 0.021 to 0.007 min^{-1}, which could be explained by the multiple reactions including radical and non-radical oxidation in this system (Fig 3e). Because of the chemical structure of SMX, the 8N atom on the benzene ring and 7S atom of the sulfonamide group could be attacked by PMS via the electrophilic and nucleophilic reactions (Boreen et al., 2004; Yin et al., 2018). The decrease of PMS decomposition rate in the presence of SMX indicated that the radical generation was inhibited (reaction to the right side of Fig 3e), which verified the existence of non-radical oxidation pathway. As shown in Fig 3e, when PMS was consumed by SMX directly, the reaction for radical generation would be inhibited, resulting a lower PMS decomposition rate (Fig 3b).

Based on these observations, other organics might also affect the PMS decomposition. To investigate the effect of natural organic matters (NOMs) on the PMS decomposition and SMX degradation, humic acid (HA) with different concentrations (0-20 mg L^{-1}) was added in the system as a surrogate of NOM. Results showed that with addition of HA, the degradation of SMX decreased which could be attributed to radical scavenging by HA (Fig S3a). However, the addition of HA also increased PMS consumption (Fig S3b). These results indicated that SMX degradation efficiency would be suppressed in the natural environment, especially in the presence of NOM.

The degradation efficiency of SMX with initial concentration range of 10-40 μM is shown in Fig S4. Before addition of PMS, the removal of SMX is negligible (±2% in 60 min). This indicates that adsorption of SMX by the catalyst is negligible. Therefore, the removal of SMX in the PMS/$CoFeO_{2.5}$ system was caused by its degradation instead of adsorption. Results in Fig S4 show that the degradation rate decreases with increased SMX initial concentration. To gain a better understanding on SMX transformation pathway in PMS/$CoFeO_{2.5}$ system, a higher initial concentration of 40 μM was chosen for the following experiments.

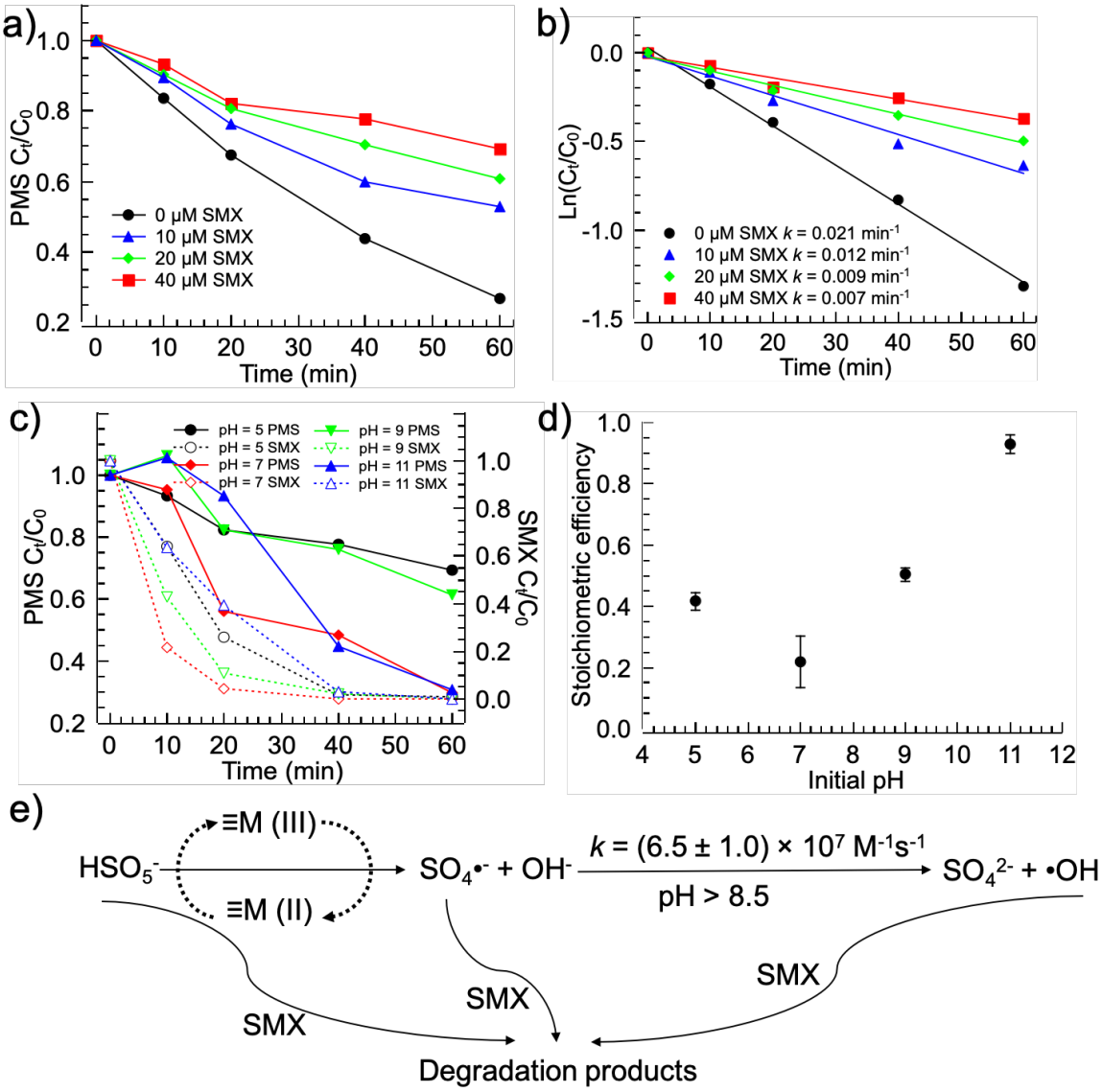

Fig 3. a-b) PMS decomposition with/without SMX in the presence of $CoFeO_{2.5}$; c-d) effect of pH on PMS and SMX degradation as well as the calculated stoichiometric efficiencies and e) the possible reactions in PMS/$CoFeO_{2.5}$/SMX system [Experimental Conditions: $CoFeO_{2.5}$ = 0.2 g L^{-1}; PMS = 0.4 mM; pH = 5 for a and b; SMX = 40 μM for c].

The stoichiometric efficiency, which is defined as the number of moles of SMX oxidized for every mole of PMS activated in the presence of $CoFeO_{2.5}$ is calculated for different pH values.

$$\eta = \Delta [SMX] / \Delta [PMS] \quad (2)$$

Fig 3d shows that the stoichiometric efficiency (calculated at the reaction time of 20 min with the initial SMX concentration of 40 μM) increased with increasing initial pH value except pH 5. At pH 7, SMX degradation shows the highest reaction rate (Fig 3c), while the stoichiometric efficiency is lower than that of pH 9 and 11 due to the high consumption of PMS at pH 7 (Eq. 2). As shown in Fig 3e, SMX could be oxidized by PMS via non-radical pathway ($^1O_2$ oxidation/direct PMS oxidation) (Yin et al., 2018), the consumption of PMS would inhibit the radical generation process due to the limiting PMS concentration (Oh et al., 2016). Meanwhile, SMX can also react with radicals produced by PMS decomposition, which would accelerate the radical generation (Fig 3e). Furthermore, sulfate radical generated via PMS decomposition would be transformed to hydroxyl radical at high pH values, which would further increase the decomposition of PMS.

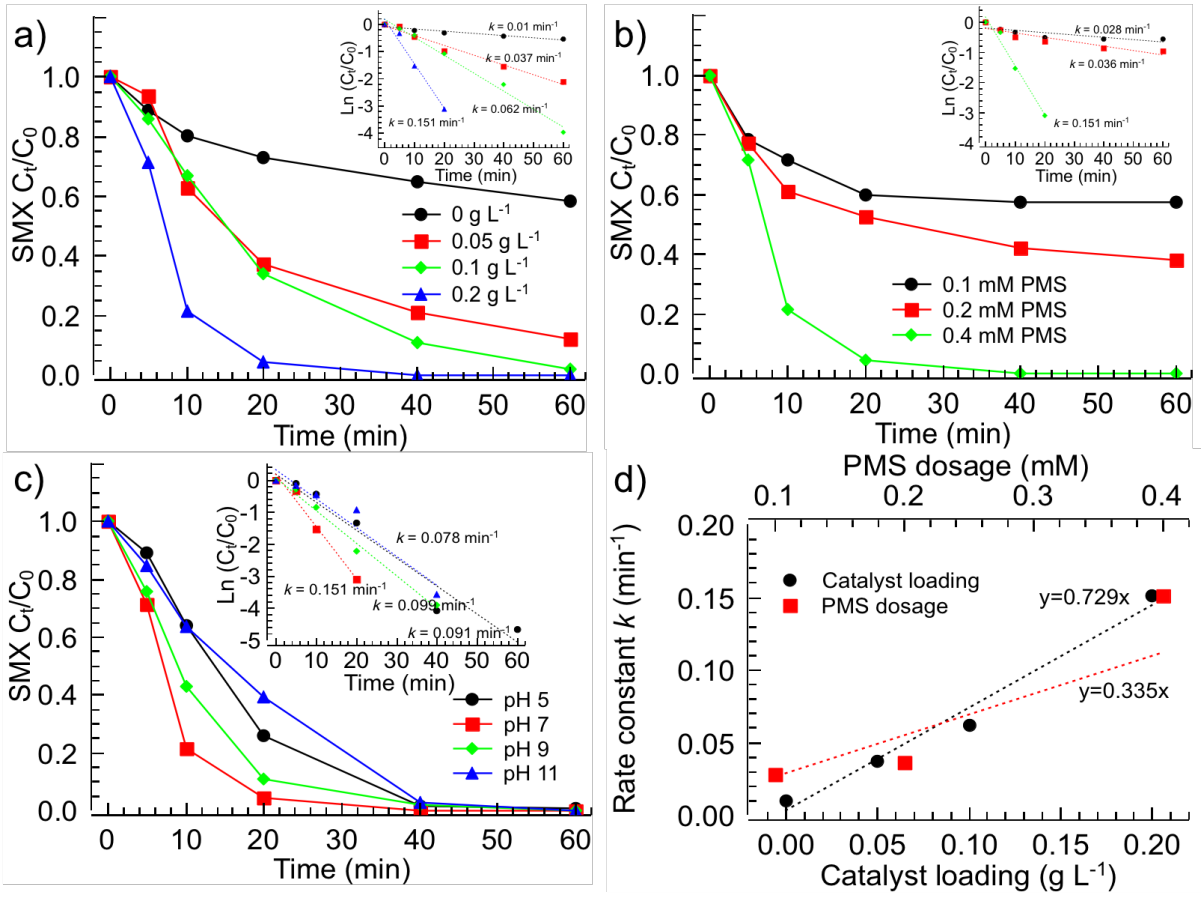

Fig 4. Effects of catalyst loading amount (a), PMS dosage (b) and pH (c) on the degradation of SMX and (d) effects of catalyst loading and PMS dosage on SMX degradation kinetic rate

constants [Experimental Conditions: a - SMX = 40 μM, PMS = 0.4 mM, pH = 7; b - SMX = 40 μM, $CoFeO_{2.5}$ = 0.2 g L^{-1}, pH = 7; c - SMX = 40 μM, PMS = 0.4 mM, $CoFeO_{2.5}$ = 0.2 g L^{-1}].

As shown in Fig 4, the SMX degradation data were fitted using the pseudo first-order kinetics (Eq.3) and the apparent rate constants are calculated and summarized in Table 2.

$$d[SMX] / dt = - k_{obs\text{-}SMX} [SMX] = - k_{SA\text{-}SMX} (C_S) [SMX] \quad (3)$$

where $k_{obs\text{-}SMX}$ represents the observed pseudo-first-order rate constant (min^{-1}) for SMX degradation, $k_{SA\text{-}SMX}$ is the SMX degradation rate constant normalized with the specific surface area (L m^{-2} min^{-1}) and Cs is the surface area of catalyst in solution (m^2 L^{-1}). Results show that SMX degradation is enhanced with the increase of catalyst loading amount which is in accordance of Cs (Fig 4a). The degradation efficiency was around 40% for at 0.4 mM PMS without $CoFeO_{2.5}$, while the removal efficiency increased to 88%, 98% and 100% for $CoFeO_{2.5}$ dosage of 0.05, 0.1 and 0.2 g L^{-1}, respectively. Meanwhile, SMX degradation also showed a positive dependence on PMS dosage. The degradation efficiency remained at 40% at 0.1 mM PMS and increased to 60% and 100% for 0.2 and 0.4 mM PMS, which shows the active sites on $CoFeO_{2.5}$ surface was not totally occupied by PMS at concentrations of less than 0.4 mM. The observed rate constant shows a liner relationship with both catalyst loading as well as PMS dosage (Fig 4d), in which the catalyst loading amount has a more significant effect. The effect of initial pH on SMX degradation was investigated by adding NaOH and the results show that the catalyst has a wide pH range tolerance (Fig 4c). All degradation efficiencies can achieve to ~100% at 40 min in the pH range of 5-11 and the pH decreased slightly (<0.5) during the reaction. The optimized condition happens at pH 7 with an observed rate constant k of 0.151min^{-1}.

Table 2. Summary on the SMX degradation kinetics with different parameters.

Parameters	$k_{obs\text{-}SMX}$ (min^{-1})	$k_{SA\text{-}SMX}$ (L m^{-2} min^{-1})	Cs (m^2 L^{-1})
$CoFeO_{2.5}$			
0 g L^{-1}	0.010	N.A.	N.A.
0.05 g L^{-1}	0.037	0.078	0.475
0.1 g L^{-1}	0.062	0.065	0.950
0.2 g L^{-1}	0.151	0.079	1.900
PMS			
0.1 mM	0.028	0.015	1.900
0.2 mM	0.036	0.019	1.900
0.4 mM	0.151	0.079	1.900
pH			
5	0.091	0.045	1.900
7	0.151	0.079	1.900
9	0.099	0.052	1.900
11	0.078	0.041	1.900

3.4 Mechanism for the radical generation

PMS could be activated by heterogeneous or homogeneous reaction to generate $SO_4\bullet^-$, •OH and $SO_5\bullet^-$. In literatures, TBA and MeOH have been widely used to indirectly indicate the presence of reactive radicals ($SO_4\bullet^-$ and •OH) in the PMS/catalyst system due to the low rate constant with $SO_5\bullet^-$ ($\leq 10^3$ M^{-1} s^{-1}) (Feng et al., 2016; Xu and Wang, 2011). Meanwhile, it has been proven that compared with $SO_4\bullet^-$ and •OH, $SO_5\bullet^-$ shows an insignificant contribution on the organic degradation (Bao et al., 2018b). However, except for the different abilities for scavenging radicals, alcohols also show the different adsorption properties onto the catalyst

and subsequent in activation of the active sites (Guan et al., 2013). Hence, it is necessary to use other scavengers to identify the reactive species in heterogeneous metal oxides catalyzed oxidation. In the present study, different chemical scavengers including TBA, MeOH, nitrobenzene (NB), phenol, benzoquinone (BQ) and NaN_3 were used as an indirect technique to identify the presence of reactive radicals. The screening of scavengers (Table S2) was performed and the details are shown in Fig S5 and S6. Results show that phenol and BQ have no significant selectivity on the radicals scavenging, while the alcohols might affect the chemical polarity of the system as well as the HPLC detection.

Based on the screening results of different scavengers, NB was selected as •OH probe compound due to its low reactivity with $SO_4^{\bullet-}$, with the rate constants of $k_{NB+\bullet OH}$ of (3.0-3.9) $\times 10^9$ M^{-1} s^{-1} and $k_{NB+SO_4^{\bullet-}}$ of $<10^6$ M^{-1} s^{-1} (Liang and Su, 2009). NaN_3 was used to quench all reactions since it has been reported to be effective for quenching •OH (1.2×10^{10} M^{-1} s^{-1}), $SO_4^{\bullet-}$ (2.51×10^9 M^{-1} s^{-1}) and non-radical oxidation process ($^1O_2$ and PMS direct oxidation) (Zhou et al., 2015). The degradation of NB verified the formation of •OH in this system (Fig 5d) and the kinetic expressions of NB and SMX degradation could be expressed as follows:

$$-dC_{NB}/dt = k_{NB+\bullet OH}\,[\bullet OH]\,C_{NB} = k_{obs\text{-}NB}\,C_{NB} \quad (4)$$

$$-dC_{SMX}/dt = k_{SMX+\bullet OH}\,[\bullet OH]\,C_{SMX} + k_{SMX+SO_4^{\bullet-}}\,[SO_4^{\bullet-}]\,C_{SMX} + k_{SMX+PMS}\,[PMS]\,C_{SMX} = k_{obs\text{-}SMX},\,C_{SMX} \quad (5)$$

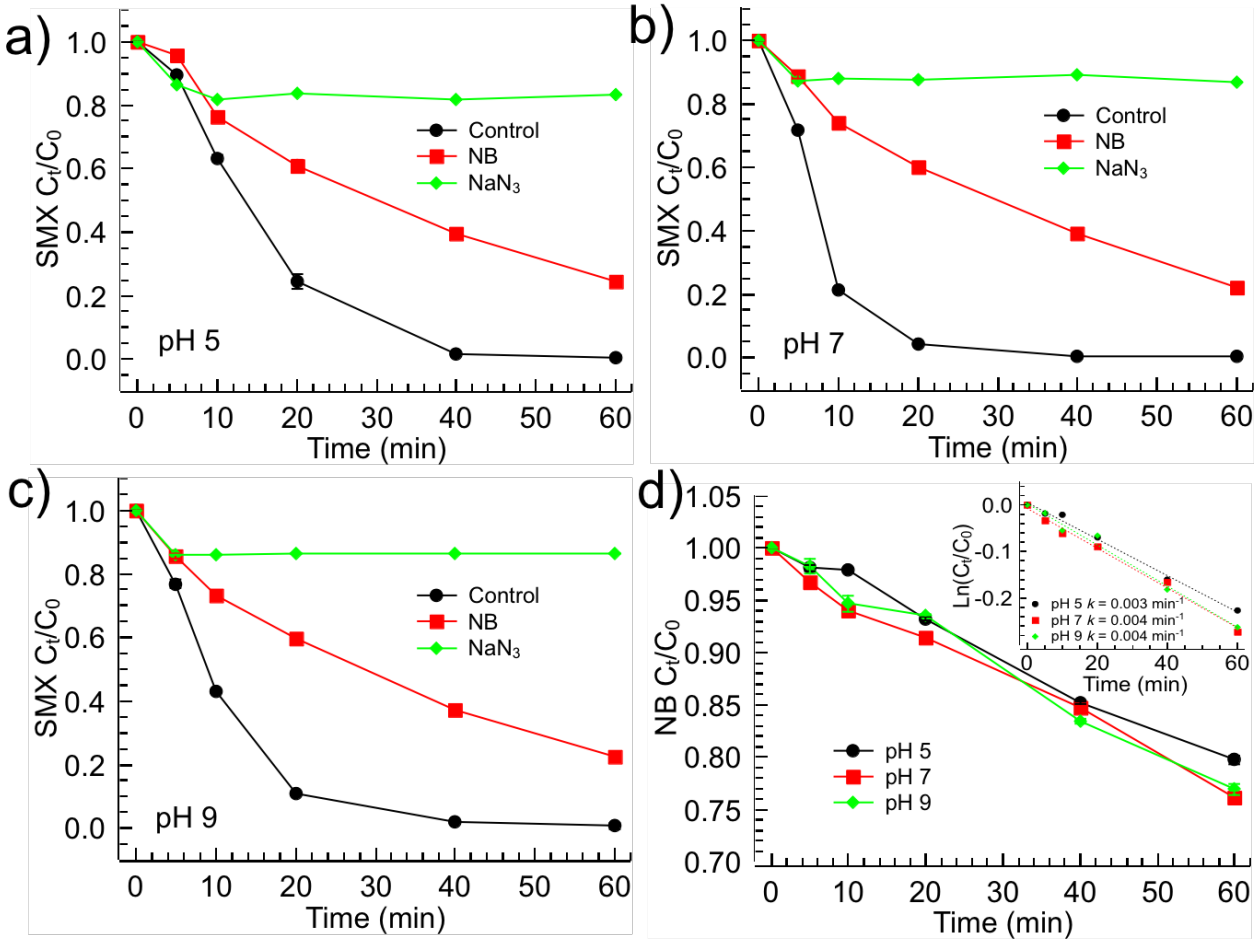

Fig 5. Effects of different scavengers on the degradation of SMX (Experimental Conditions: [SMX] = 40 μM; [PMS] = 0.4 mM; [$CoFeO_{2.5}$] = 0.2 g L^{-1}; [NB] = 10 mg L^{-1} and [NaN_3] = 5 mM).

The degradation of SMX without $CoFeO_{2.5}$ shows the non-radical pathway (e.g. PMS direct oxidation and $^1O_2$ oxidation) with a rate constant k of 0.01 min^{-1} (Fig 4a). In this work, due to the high reactivity of radicals, we assumed that $k_{SMX+PMS}$ is much less significant compared with those of $k_{SMX+\bullet OH}$ ((8.5±0.3) × 10^9 M^{-1} s^{-1}) and $k_{SMX+SO_4^{\bullet-}}$ (12.5× 10^9 M^{-1} s^{-1}). The inhibition on SMX degradation rate constants by NB verified the role of •OH in the degradation process. In the presence of NB, •OH can react with both SMX (1) and NB (2) at the calculated rate constants of k_1= $k_{SMX+\bullet OH}$ (8.5±0.3) × 10^9 M^{-1} s^{-1}) × C_{SMX} (0.04 mM) = 0.34 × 10^6 s^{-1}, k_2 = $k_{NB+\bullet OH}$ (3.0-3.9) × 10^9 M^{-1} s^{-1} × C_{NB} (10 mg L^{-1}) = 0.28 × 10^6 s^{-1}. Therefore, the

possibility of hydroxyl radical to react with NB is assumed as P = $0.28 \times 10^6/(0.28+0.34) \times 10^6$ = 45%. The calculated •OH generation increased from $(1.03\text{-}1.33) \times 10^{-10}$ M to $(1.37\text{-}1.78) \times 10^{-10}$ M when the initial pH increased from 5 to 9 (Eq. 4). Under higher pH, SO_4•$^-$ would decompose to •OH (Fig 3e), increasing the •OH concentration.

Table 3. The calculated observed reaction rate constants k_{obs} in SMX/NB system (a) and SMX system (b) (Experimental Conditions: [SMX] = 40 μM; [PMS] = 0.4 mM; [$CoFeO_{2.5}$] = 0.2 g L^{-1} and [NB] = 10 mg L^{-1}).

pH	$k_{obs\text{-}NB}$ (min^{-1}) [a]	$k_{obs\text{-}SMX'}$ (min^{-1}) [a]	$k_{obs\text{-}SMX}$ (min^{-1}) [b]
5	0.003	0.023	0.091
7	0.004	0.025	0.151
9	0.004	0.025	0.099

Table 3 shows that NB exhibits the inhibition on the SMX degradation in all pH ranges (5-9), which verified the role of •OH on SMX degradation. If we assumed that •OH is the only functional radical, $k_{obs\text{-}SMX'}/k_{obs\text{-}NB}$ should be around 2-3 (Eqs. 4-5). However, the calculated value of $k_{obs\text{-}SMX'}/k_{obs\text{-}NB}$ is in the range of 6-8 (Table 3), indicating the other contributions (non-radical pathway as well as other radical pathway, i.e., SO_4•$^-$) on SMX degradation.

To further identify the radicals generated in PMS/$CoFeO_{2.5}$/SMX system, an attempt with EPR experiments was conducted. There were no obvious characteristic signals present in the EPR spectra of experiments conducted without catalyst (Fig S7). However, spin trapping adducts DMPO-•OH and DMPO-SO_4•$^-$ were identified when catalyst was introduced (Fig 6a), suggesting that the as-prepared catalyst could effectively activate PMS to generate radicals (Wang et al., 2016). Meanwhile, •OOH was also detected in this system when BMPO was used as the spin trapping agent (Fig 6a) and the detection of $^1O_2$ further confirmed the non-radical pathway of SMX degradation (Fig 6b).

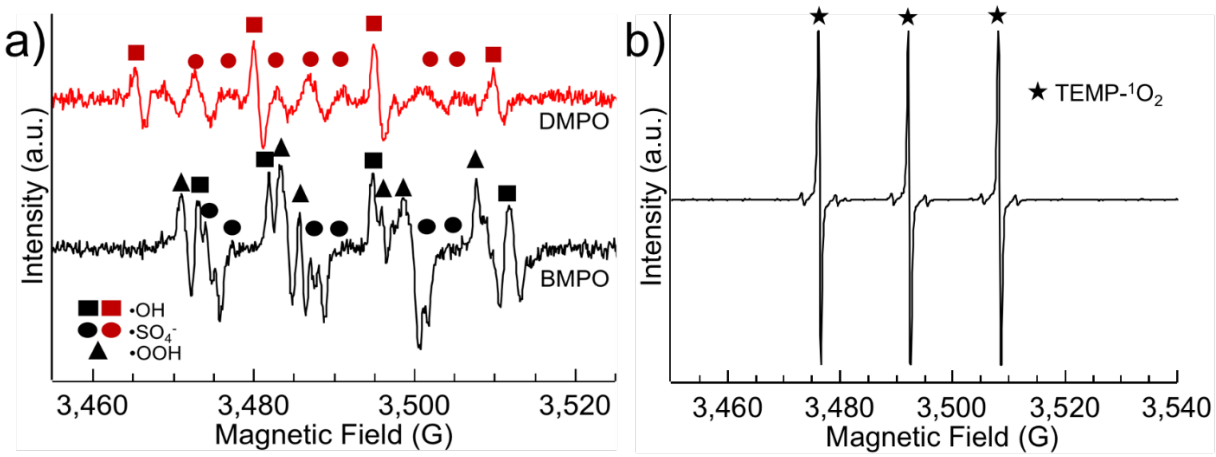

Fig 6. EPR spectra in activation of PMS with different spin trapping agents in the presence of the as-prepared catalyst.

3.5 Proposed SMX transformation pathways in PMS/$CoFeO_{2.5}$ system

Based on the radical scavenger experiments and EPR results, both non-radical pathway and radical pathway are involved in the SMX degradation processes. Through the identification of oxidation products, the possible transformation pathways for SMX oxidation in PMS/$CoFeO_{2.5}$ system is proposed in Fig 7. The main transformation products from SMX degradation are summarized in Table S3 and Fig S8. In the transformation process, three major transformation pathways are proposed to occur simultaneously: 1) oxidation of the amine group on the benzene ring to yield the nitro-SMX derivative; 2) hydroxylation of the benzene and isoxazole rings; and 3) cleavage of the sulfonamide bond.

In the non-radical oxidation pathway, PMS played a role as inorganic oxidizer that can react with SMX through both electrophilic and nucleophilic reactions. Meanwhile, $^1O_2$ which could be generated via PMS decomposition might also affect the SMX transformation. However, due to the limited amount of $^1O_2$, PMS direct oxidation on SMX transformation should be the dominant non-radical oxidant pathway (Yin et al., 2018). As reported, the density functional theory (DFT) calculation confirmed PMS non-radical oxidation, in which the N atom on the benzene ring and S atom of the sulfanilamide group could be selectively attacked by PMS direct oxidation. The results show that the 8N atom on the benzene ring is the most

susceptible sites to be attacked by PMS to form nitroso- or nitro group adducted SMX in the electrophilic oxidation (Yin et al., 2018). During the transformation process, SMX exhibited a color changes from colorless to yellow and back to colorless over extended time periods. Considering the chromogenic properties of the dyes, the nitro group is an efficient functional group for light absorption. Thus, SMX could be degraded through the attack of 8N atom via non-radical pathway to generate the products P1 and P2. In the nucleophilic reaction, the DFT calculation shows that 7S atom of the sulfonamide group was the most vulnerable site which could be attacked by nucleophilic species to break down the functional groups (Boreen et al., 2004; Yin et al., 2017). The possible products formed by attacking the S atom of SMX were detected as P5 and P11. Meanwhile, the isomerization reaction of isoxazole ring on the SMX could also occur in the non-radical pathway, resulting in the rearrangement of isoxazole ring on the SMX (P3). This was also reported in permanganate oxidation and photodegradation of SMX (Gao et al., 2014; Trovó et al., 2009). It is suggested that P11 would further undergo a reaction from the addition of hydroxyl group on the benzene ring (P12) and the loss of the SO_2 group (P13) followed by the substitution of $–NH_2$ group (P14).

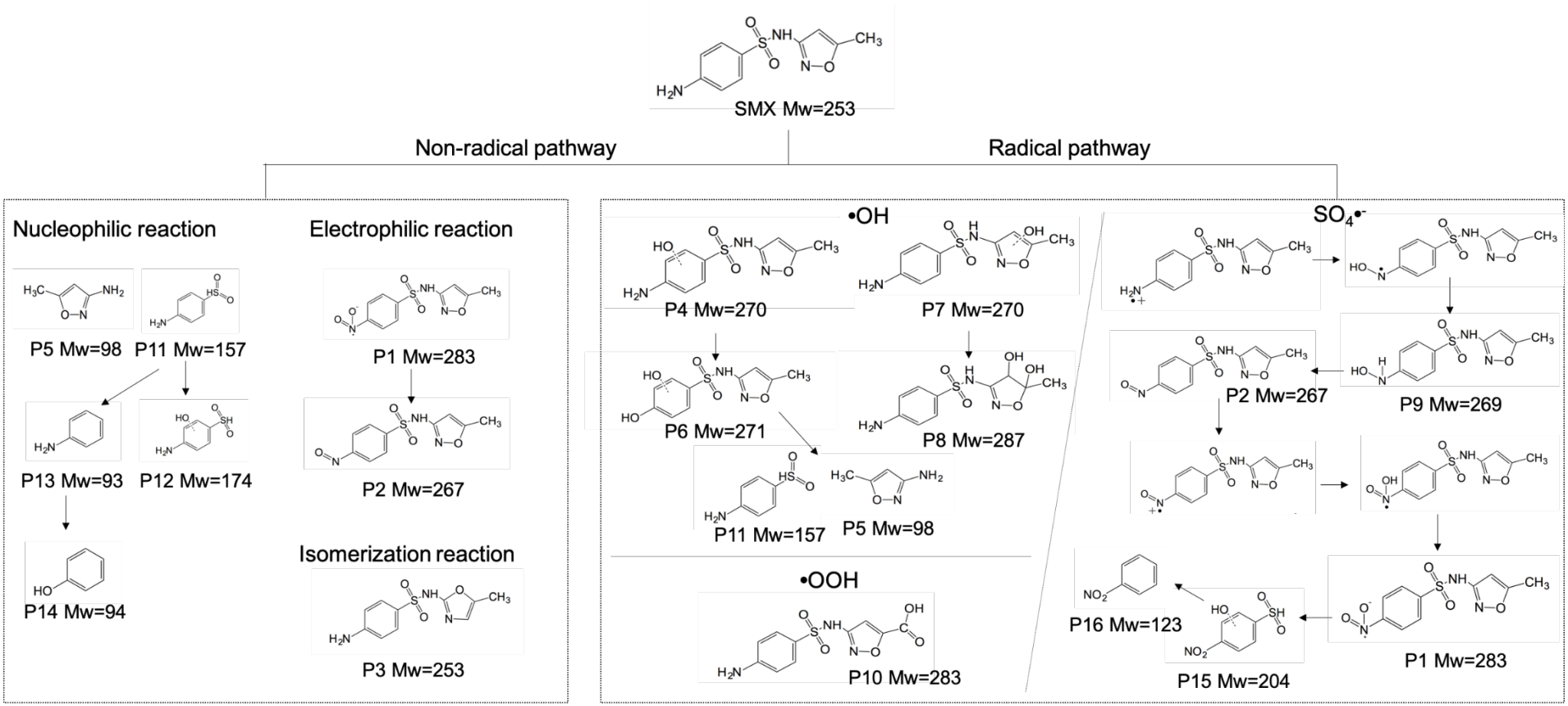

Fig 7. Proposed SMX transformation pathways in PMS system in the presence of $CoFeO_{2.5}$.

In the radical pathway, three radicals (i.e., $SO_4\bullet^-$, •OH and •OOH) were detected and functionalized in this system. $SO_4\bullet^-$ has a highly-selective electrophile mainly acting by electron-transfer from N to $SO_4\bullet^-$ yielding to a N-centered radical as a first intermediate. This radical cation underwent a fast-reversible hydration to yield an aniline radical, which was further neutralized by molecular oxygen probably leading to hydroxylamine (P9) and nitroso derivatives (P2), which were readily hydrolyzed into nitro-SMX (P1) (Ahmed et al., 2012). The nitro-SMX could be furthered oxidized to become P15 and P16 via the broken of S-N functional bond. Thus, $SO_4\bullet^-$ would attack -NH_2 group more efficiently and favor the formation of nitrogen oxidized products. Different from the $SO_4\bullet^-$ pathway, •OH exhibits high reactivity with olefinic double bonds and anilines (Buxton et al., 1988), therefore, the radical addition on the benzene and isoxazole rings was commonly observed as the first step to generate products (P4 and P7) in •OH transformation pathway. The •OH can further oxidize the double bond C=C on the isoxazole ring to yield a tertiary carbon-centered radical, with can react with oxygen to generate a peroxy radical. This peroxy radical can abstract a hydrogen from a donor and form the corresponding hydroperoxide, which can produce a hydroxyl radical and an alkoxy radical to form dihydroxylated SMX (P8) via hydrogen abstraction (Hu et al., 2007; Yang et al., 2017). P6 could be generated by the substitution of -NH_2 group with hydroxyl group. Meanwhile, the hydroxyl radicals can also attack the 7S atom to break down the S-N bond to generate the products of P5 and P11 (similar with the nucleophilic pathway). Furthermore, it is proposed that carboxylic acid group (P10) might be formed due to the oxidation at the methyl group on the isoxzaole ring via •OOH radical, which can be exist as superoxide ion in higher pH (Eq.6).

$$\bullet OOH + OH^- \leftrightarrow \bullet O_2^- + H_2O \qquad (pK_b = 9.12) \qquad (6)$$

3.6 Mechanism of PMS activation in the presence of $CoFeO_{2.5}$

The chemical bonding between $CoFeO_{2.5}$ and PMS was investigated by FTIR (Fig S9). The peaks at the region of 900-1340 cm^{-1} for PMS alone are generally assigned to the symmetric and asymmetric stretching of the S-O bonds (Gonzalez et al., 2010). However, a slightly blue-shift was observed when $CoFeO_{2.5}$ was added into PMS solution suggesting the change of S-O bond.

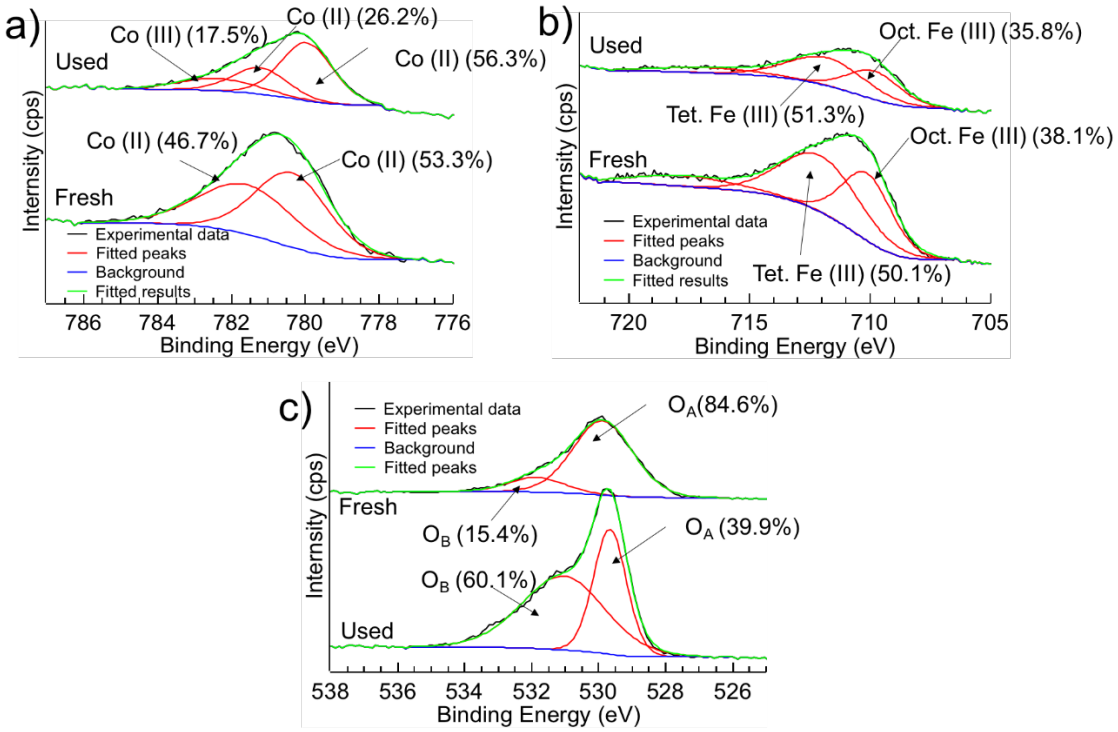

Fig 8. XPS spectra of $CoFeO_{2.5}$ before and after the reaction in PMS/$CoFeO_{2.5}$/SMX system.

To explore the PMS activation mechanism, the XPS spectra of the $CoFeO_{2.5}$ before and after the reaction were analyzed. The binding energies and relative intensities are summarized in Fig 8. The deconvoluted Fe 2p3/2 spectrum displayed three peaks with binding energies at 710.1, 712.1 and 717.6 eV, which could be assigned to octahedral Fe (III), tetrahedral Fe (III) and satellite Fe (III), respectively (Fig 8b) (Petran et al., 2016). After the reaction, the ratio of different Fe states changed marginally (< 5%), indicating that no significant redox reaction has occurred for iron. As shown in Fig 8a, two peaks with binding energy appearing at 780.4 and

781.6 eV are ascribed to Co^{2+} ions in octahedral and tetrahedral sites with the relative contributions to the overall Co are 53.3% and 46.7%, respectively. However, the Co 2p3/2 peak is composed of three peaks at 780.0, 781.2 and 782.4 eV, with relative contributions to the overall Co intensity of 56.3% 26.2% and 17.5%, respectively, which is ascribed to Co^{2+} in octahedral sites, tetrahedral sites and Co^{3+} in octahedral sites (Zhou et al., 2008). The results show that the active site in this process is Co, which is mainly present in +2 valent state before reaction and undergoes a partial increase to +3 valent state after catalytic reaction. The oxidizing reaction occurs on the surface and Co^{2+} would provide the electrons in order to keep the balance of charge on the catalyst surface, meanwhile Co^{3+} will accept the electrons from the system, resulting the Co^{2+}-Co^{3+}-Co^{2+} redox process in the system (Fig 9). The high-resolution O1s spectra are deconvoluted into two peaks at 529 and 531 eV, which are assigned to the lattice oxygen (O_A) and surface hydroxyl species (O_B). After reaction, it is found out that the O_A decreased from 84.6 to 39.9%, which should be accompanied with the oxidation reaction from Co^{2+} to Co^{3+} (Ren et al., 2015). Meanwhile, the metal leaching results show that Fe shows a much less leaching compared with Co (Table 1). Therefore, in this system, it was proposed that Co works as the active site while Fe works as the adsorption site since the surface area of nano-bimetallic oxides increased with increasing of Fe amount (Fig 2b), the similar results could be found in the previous study (Huang et al., 2017).

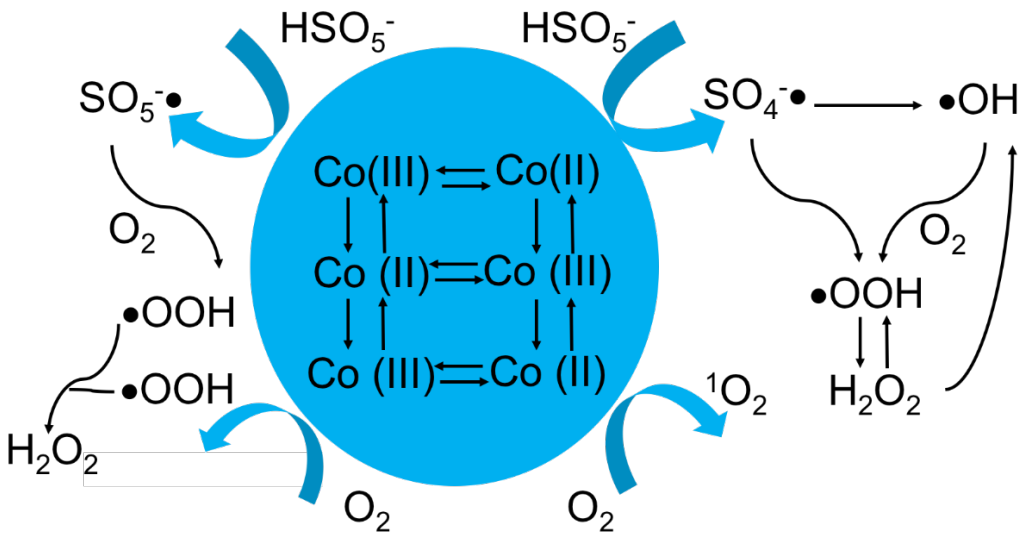

Fig 9. The radical generation mechanism via PMS activation in the presence of $CoFeO_{2.5}$.

Therefore, these results confirm that Co^{2+} donated electrons to PMS and initiated its decomposition (Eq.7). Co^{3+} was then reduced by HSO_5^- to complete the redox cycles (Eq.8), resulting in the continuous reaction (Anipsitakis and Dionysiou, 2004; Oh et al., 2016). In this process, •OH could be generated through the reaction between $SO_4•^-$ and H_2O/OH^- (Eqs. 9 and 10) and can react with HSO_5^- to produce $SO_5•^-$ (Eq. 11) (Hayon et al., 1972; Norman et al., 1970). Based on the EPR results, •OOH was proposed to be formed via the reaction of $SO_4•^-$/•OH and H_2O/O_2 (Fig 9). •OOH could react to produce H_2O_2, which can further generate radicals in the presence of catalyst (Sehested et al., 1968). Meanwhile, $^1O_2$ can be produced by O_2 in the presence of radicals (Daimon et al., 2008).

$$HSO_5^- + Co\ (II) \rightarrow SO_4•^- + Co\ (III) + OH^- \quad (7)$$

$$HSO_5^- + Co\ (III) \rightarrow SO_5•^- + Co\ (II) + H^+ \quad (8)$$

$$SO_4•^- + H_2O \rightarrow SO_4^{2-} + •OH + H^+ \text{ (over the entire pH range) } k[H_2O] < 3 \times 10^3\ s^{-1} \quad (9)$$

$$SO_4•^- + OH^- \rightarrow SO_4^{2-} + •OH \text{ (alkaline media) } k = (6.5\pm1.0) \times 10^7\ M^{-1}\ s^{-1} \quad (10)$$

$$HSO_5^- + •OH \rightarrow SO_5•^- + H_2O \quad k = 2.9 \times 10^8\ M^{-1}\ s^{-1} \quad (11)$$

Furthermore, the stability test of $CoFeO_{2.5}$ to activate PMS for SMX degradation was investigated. The catalyst was recycled by magnetic assisted centrifugation and the reusability test showed the degradation efficiency could be maintained at >95% after five cycles (Fig S10).

4. Conclusion

A series of nano-bimetallic Co/Fe oxides with different stoichiometric ratios were prepared and used for the heterogeneous activation of PMS for SMX degradation. Based on the results presented, the following conclusions can be drawn:

1) Nano-bimetallic Co/Fe oxides with different stoichiometric ratios could be prepared via a one-step combustion method.
2) The as-prepared catalyst of $CoFeO_{2.5}$ shows the highest stability and the stoichiometric efficiency in PMS/$CoFeO_{2.5}$/SMX system has a positive relationship with initial pH value.
3) The EPR results and chemical quenching experiments confirmed the generation of multiple radicals or reactive oxygen species (i.e., $SO_4\bullet^-$, •OH, •OOH and $^1O_2$).
4) The transformation of SMX in PMS/$CoFeO_{2.5}$ system includes both radical pathway and non-radical pathway, in which radical pathway ($SO_4\bullet^-$ and •OH) plays a major role.
5) The change of S-O bond showed the generation of radicals from PMS oxidation and the XPS spectra of $CoFeO_{2.5}$ before and after reaction demonstrated the electron transfer between PMS and $CoFeO_{2.5}$.
6) Based on the XPS and ICP results, it could be hypothesized that Fe functioned as the absorption site while Co functioned as the active site in the catalyst.

Overall, a comprehensive transformation of SMX in PMS/$CoFeO_{2.5}$ system was explored in this study. Meanwhile, the one-step combustion method could be used for the nano-bimetallic oxides preparation which could be applied for the water treatment.

Reference

Ahmed, M.M., Barbati, S., Doumenq, P., Chiron, S., 2012. Sulfate radical anion oxidation of diclofenac and sulfamethoxazole for water decontamination. Chem. Eng. J. 197, 440–447.

Alexy, R., Kümpel, T., Kümmerer, K., 2004. Assessment of degradation of 18 antibiotics in the closed bottle test. Chemosphere 57, 505–512.

Anipsitakis, G.P., Dionysiou, D.D., 2004. Radical generation by the interaction of transition metals with common oxidants. Environ. Sci. Technol. 38, 3705–3712.

Anipsitakis, G.P., Stathatos, E., Dionysiou, D.D., 2005. Heterogeneous activation of oxone using Co_3O_4. J. Phys. Chem. B 109, 13052–13055.

Bao, Y., Lim, T.-T., Wang, R., Webster, R.D., Hu, X., 2018a. Urea-assisted one-step synthesis of cobalt ferrite impregnated ceramic membrane for sulfamethoxazole degradation via peroxymonosulfate activation. Chem. Eng. J. 343, 737–747.

Bao, Y., Oh, W.-D., Lim, T.-T., Wang, R., Webster, R.D., Hu, X., 2018b. Surface-nucleated heterogeneous growth of zeolitic imidazolate framework–A unique precursor towards catalytic ceramic membranes: Synthesis, characterization and organics degradation. Chem. Eng. J. 353, 69–79.

Boreen, A.L., Arnold, W.A., McNeill, K., 2004. Photochemical fate of sulfa drugs in the aquatic environment: sulfa drugs containing five-membered heterocyclic groups. Environ. Sci. Technol. 38, 3933–3940.

Buxton, G.V., Greenstock, C.L., Helman, W.P., Ross, A.B., 1988. Critical review of rate constants for reactions of hydrated electrons, hydrogen atoms and hydroxyl radicals ($\cdot OH/\cdot O^-$ in aqueous solution. J. Phys. Chem. Ref. Data 17, 513–886.

Chen, L., Zuo, X., Zhou, L., Huang, Y., Yang, S., Cai, T., Ding, D., 2018. Efficient heterogeneous activation of peroxymonosulfate by facilely prepared Co/Fe bimetallic oxides: Kinetics and mechanism. Chem. Eng. J. 345, 364–374.

Costa, R.C., Lelis, M.F.F., Oliveira, L.C.A., Fabris, J.D., Ardisson, J.D., Rios, R., Silva, C.N., Lago, R.M., 2006. Novel active heterogeneous Fenton system based on $Fe_{3-x}M_xO_4$ (Fe, Co, Mn, Ni): the role of M^{2+} species on the reactivity towards H_2O_2 reactions. J. Hazard. Mater. 129, 171–178.

Daimon, T., Hirakawa, T., Kitazawa, M., Suetake, J., Nosaka, Y., 2008. Formation of singlet molecular oxygen associated with the formation of superoxide radicals in aqueous suspensions of TiO_2 photocatalysts. Appl. Catal. Gen. 340, 169–175.

Eberson, L., 1982. Electron-transfer reactions in organic chemistry. Adv. Phys. Org. Chem. 18, 79–185.

Fang, G.-D., Dionysiou, D.D., Wang, Y., Al-Abed, S.R., Zhou, D.-M., 2012. Sulfate radical-based degradation of polychlorinated biphenyls: effects of chloride ion and reaction kinetics. J. Hazard. Mater. 227, 394–401.

Feng, Y., Wu, D., Deng, Y., Zhang, T., Shih, K., 2016. Sulfate radical-mediated degradation of sulfadiazine by $CuFeO_2$ rhombohedral crystal-catalyzed peroxymonosulfate: synergistic effects and mechanisms. Environ. Sci. Technol. 50, 3119–3127.

Gao, S., Zhao, Z., Xu, Y., Tian, J., Qi, H., Lin, W., Cui, F., 2014. Oxidation of sulfamethoxazole (SMX) by chlorine, ozone and permanganate—a comparative study. J. Hazard. Mater. 274, 258–269.

Ghanbari, F., Moradi, M., 2017. Application of peroxymonosulfate and its activation methods for degradation of environmental organic pollutants. Chem. Eng. J. 310, 41–62.

Godfrey, E., Woessner, W.W., Benotti, M.J., 2007. Pharmaceuticals in On-Site Sewage Effluent and Ground Water, Western Montana. Groundwater 45, 263–271.

530 Gonzalez, J., Torrent-Sucarrat, M., Anglada, J.M., 2010. The reactions of SO_3 with HO_2 radical and
531 $H_2O^{\cdots}$ HO_2 radical complex. Theoretical study on the atmospheric formation of HSO_5 and H_2
532 SO_4. Phys. Chem. Chem. Phys. 12, 2116–2125.
533 Guan, Y.-H., Ma, J., Ren, Y.-M., Liu, Y.-L., Xiao, J.-Y., Lin, L., Zhang, C., 2013. Efficient degradation
534 of atrazine by magnetic porous copper ferrite catalyzed peroxymonosulfate oxidation via the
535 formation of hydroxyl and sulfate radicals. Water Res. 47, 5431–5438.
536 Hayon, E., Treinin, A., Wilf, J., 1972. Electronic spectra, photochemistry, and autoxidation mechanism
537 of the sulfite-bisulfite-pyrosulfite systems. SO_2^-, SO_3^-, SO_4^-, and SO_5^-radicals. J. Am. Chem.
538 Soc. 94, 47–57.
539 Hu, L., Flanders, P.M., Miller, P.L., Strathmann, T.J., 2007. Oxidation of sulfamethoxazole and related
540 antimicrobial agents by TiO_2 photocatalysis. Water Res. 41, 2612–2626.
541 Hu, P., Long, M., 2016. Cobalt-catalyzed sulfate radical-based advanced oxidation: a review on
542 heterogeneous catalysts and applications. Appl. Catal. B Environ. 181, 103–117.
543 Huang, G.-X., Wang, C.-Y., Yang, C.-W., Guo, P.-C., Yu, H.-Q., 2017. Degradation of bisphenol A by
544 peroxymonosulfate catalytically activated with $Mn_{1.8}Fe_{1.2}O_4$ nanospheres: synergism between
545 Mn and Fe. Environ. Sci. Technol. 51, 12611–12618.
546 Jansomboon, W., Boontanon, S.K., Boontanon, N., Polprasert, C., Da, C.T., 2016. Monitoring and
547 determination of sulfonamide antibiotics (sulfamethoxydiazine, sulfamethazine,
548 sulfamethoxazole and sulfadiazine) in imported Pangasius catfish products in Thailand using
549 liquid chromatography coupled with tandem mass spectrometry. Food Chem. 212, 635–640.
550 Li, C., Wu, J., Peng, W., Fang, Z., Liu, J., 2019. Peroxymonosulfate activation for efficient
551 sulfamethoxazole degradation by Fe_3O_4/β-FeOOH nanocomposites: Coexistence of radical and
552 non-radical reactions. Chem. Eng. J. 356, 904–914.
553 Li, Y., He, H., Fu, W., Mu, C., Tang, X.-Z., Liu, Z., Chi, D., Hu, X., 2016. In-grown structure of NiFe
554 mixed metal oxides and CNT hybrid catalysts for oxygen evolution reaction. Chem. Commun.
555 52, 1439–1442.
556 Liang, C., Su, H.-W., 2009. Identification of sulfate and hydroxyl radicals in thermally activated
557 persulfate. Ind. Eng. Chem. Res. 48, 5558–5562.
558 Liang, Y.N., Li, Y., Ang, C., Shen, Y., Chi, D., Hu, X., 2014. Novel Low Temperature Synthesis Route
559 for Functional Au/ZnFe Mixed Oxide Nanohybrids. ACS Appl. Mater. Interfaces 6, 12406–
560 12412.
561 Lindberg, R., Jarnheimer, P.AAke, Olsen, B., Johansson, M., Tysklind, M., 2004. Determination of
562 antibiotic substances in hospital sewage water using solid phase extraction and liquid
563 chromatography/mass spectrometry and group analogue internal standards. Chemosphere 57,
564 1479–1488.
565 Liu, H., Bruton, T.A., Doyle, F.M., Sedlak, D.L., 2014. In situ chemical oxidation of contaminated
566 groundwater by persulfate: decomposition by Fe (III)-and Mn (IV)-containing oxides and
567 aquifer materials. Environ. Sci. Technol. 48, 10330–10336.
568 Miao, D., Peng, J., Wang, M., Shao, S., Wang, L., Gao, S., 2018. Removal of atorvastatin in water
569 mediated by CuFe2O4 activated peroxymonosulfate. Chem. Eng. J. 346, 1–10.
570 Nikolaou, A., Meric, S., Fatta, D., 2007. Occurrence patterns of pharmaceuticals in water and
571 wastewater environments. Anal. Bioanal. Chem. 387, 1225–1234.
572 Norman, R.O.C., Storey, P.M., West, P.R., 1970. Electron spin resonance studies. Part XXV. Reactions
573 of the sulphate radical anion with organic compounds. J. Chem. Soc. B Phys. Org. 1087–1095.
574 Oh, W.-D., Chang, V.W., Lim, T.-T., 2017. A comprehensive performance evaluation of heterogeneous
575 $Bi_2Fe_4O_9$/peroxymonosulfate system for sulfamethoxazole degradation. Environ. Sci. Pollut.
576 Res. 1–10.
577 Oh, W.-D., Dong, Z., Lim, T.-T., 2016. Generation of sulfate radical through heterogeneous catalysis
578 for organic contaminants removal: Current development, challenges and prospects. Appl. Catal.
579 B Environ. 194, 169–201.
580 Oh, W.-D., Lua, S.-K., Dong, Z., Lim, T.-T., 2014. High surface area DPA-hematite for efficient
581 detoxification of bisphenol A via peroxymonosulfate activation. J. Mater. Chem. A 2, 15836–
582 15845.
583 Petran, A., Radu, T., Culic, B., Turcu, R., 2016. Tailoring the properties of magnetite nanoparticles
584 clusters by coating with double inorganic layers. Appl. Surf. Sci. 390, 1–6.

585 Ren, Y., Lin, L., Ma, J., Yang, J., Feng, J., Fan, Z., 2015. Sulfate radicals induced from
586 peroxymonosulfate by magnetic ferrospinel MFe_2O_4 (M= Co, Cu, Mn, and Zn) as
587 heterogeneous catalysts in the water. Appl. Catal. B Environ. 165, 572–578.
588 Rizzo, L., Manaia, C., Merlin, C., Schwartz, T., Dagot, C., Ploy, M.C., Michael, I., Fatta-Kassinos, D.,
589 2013. Urban wastewater treatment plants as hotspots for antibiotic resistant bacteria and genes
590 spread into the environment: a review. Sci. Total Environ. 447, 345–360.
591 Ryan, C.C., Tan, D.T., Arnold, W.A., 2011. Direct and indirect photolysis of sulfamethoxazole and
592 trimethoprim in wastewater treatment plant effluent. Water Res. 45, 1280–1286.
593 Segura, P.A., François, M., Gagnon, C., Sauvé, S., 2009. Review of the occurrence of anti-infectives in
594 contaminated wastewaters and natural and drinking waters. Environ. Health Perspect. 117, 675.
595 Sehested, K., Rasmussen, O.L., Fricke, H., 1968. Rate constants of OH with HO_2, O_2^-, and $H_2O_2^+$ from
596 hydrogen peroxide formation in pulse-irradiated oxygenated water. J. Phys. Chem. 72, 626–
597 631.
598 Trovó, A.G., Nogueira, R.F., Agüera, A., Fernandez-Alba, A.R., Sirtori, C., Malato, S., 2009.
599 Degradation of sulfamethoxazole in water by solar photo-Fenton. Chemical and toxicological
600 evaluation. Water Res. 43, 3922–3931.
601 Wang, Y., Ao, Z., Sun, H., Duan, X., Wang, S., 2016. Activation of peroxymonosulfate by
602 carbonaceous oxygen groups: experimental and density functional theory calculations. Appl.
603 Catal. B Environ. 198, 295–302.
604 Xu, L., Wang, J., 2011. A heterogeneous Fenton-like system with nanoparticulate zero-valent iron for
605 removal of 4-chloro-3-methyl phenol. J. Hazard. Mater. 186, 256–264.
606 Yang, Y., Lu, X., Jiang, J., Ma, J., Liu, G., Cao, Y., Liu, W., Li, J., Pang, S., Kong, X., 2017.
607 Degradation of sulfamethoxazole by UV, UV/H_2O_2 and UV/persulfate (PDS): formation of
608 oxidation products and effect of bicarbonate. Water Res. 118, 196–207.
609 Yin, R., Guo, W., Du, J., Zhou, X., Zheng, H., Wu, Q., Chang, J., Ren, N., 2017. Heteroatoms doped
610 graphene for catalytic ozonation of sulfamethoxazole by metal-free catalysis: Performances and
611 mechanisms. Chem. Eng. J. 317, 632–639.
612 Yin, R., Guo, W., Wang, H., Du, J., Zhou, X., Wu, Q., Zheng, H., Chang, J., Ren, N., 2018. Selective
613 degradation of sulfonamide antibiotics by peroxymonosulfate alone: Direct oxidation and
614 nonradical mechanisms. Chem. Eng. J. 334, 2539–2546.
615 Yun, E.-T., Lee, J.H., Kim, J., Park, H.-D., Lee, J., 2018. Identifying the Nonradical Mechanism in the
616 Peroxymonosulfate Activation Process: Singlet Oxygenation Versus Mediated Electron
617 Transfer. Environ. Sci. Technol.
618 Zhang, B.-T., Zhang, Y., Teng, Y., Fan, M., 2015. Sulfate radical and its application in decontamination
619 technologies. Crit. Rev. Environ. Sci. Technol. 45, 1756–1800.
620 Zhou, Y., Jiang, J., Gao, Y., Ma, J., Pang, S.-Y., Li, J., Lu, X.-T., Yuan, L.-P., 2015. Activation of
621 peroxymonosulfate by benzoquinone: a novel nonradical oxidation process. Environ. Sci.
622 Technol. 49, 12941–12950.
623 Zhou, Z., Zhang, Y., Wang, Z., Wei, W., Tang, W., Shi, J., Xiong, R., 2008. Electronic structure studies
624 of the spinel $CoFe_2O_4$ by X-ray photoelectron spectroscopy. Appl. Surf. Sci. 254, 6972–6975.
625